J. Eur. Opt. Society-Rapid Publ. 2024, **20**, 27

https://doi.org/10.1051/jeos/2024021
Available online at: https://jeos.edpsciences.org

Journal of the European Optical Society-Rapid Publications

EOSAM 2023
Guest editors: Patricia Segonds, Guy Millot and Bertrand Kibler

RESEARCH ARTICLE

OPEN ACCESS

The role of absorption mechanism on the optimization of processing commercial polymers under high repetition rate femtosecond laser irradiation

Andrés P. Bernabeu[1,2], Guillem Nájar[1,2], Alberto Ruiz[1], Juan C. Bravo[1,2], Manuel G. Ramirez[1,2], Sergi Gallego[1,2], Andrés Márquez[1,2], and Daniel Puerto[1,2,*]

[1] I.U. Física Aplicada a las Ciencias y las Tecnologías, Universidad de Alicante, 03690 San Vicente del Raspeig, Spain
[2] Departamento de Física, Ingeniería de Sistemas y Teoría de la Señal, Universidad de Alicante, 03690 San Vicente del Raspeig, Spain

Received 29 January 2024 / Accepted 17 April 2024

Abstract. The response of three of the most used commercial polymers (poly(vinyl chloride) (PVC), poly (ethylene terephthalate) (PET) and polypropylene (PP)) under irradiation with high repetition rate (1 kHz–1 MHz) femtosecond (450 fs) multi-pulse ($N = 10$–1500) laser at $\lambda = 343$ nm, 515 nm (1.40 J/cm^2 for both former wavelengths) and 1030 nm (1.70 J/cm^2) is reported, obtaining a study on how the absorption mechanism influences the processing efficiency for these materials. Tunable ablation depth and diameters are accomplished by modifying repetition rates at a constant fluence and number of pulses. The results highlight the role of absorption mechanism, repetition rate ranges and thermal properties of the materials for benefiting ablation efficiency. Furthermore, the use of high repetition rates improves the laser processing, reducing extended thermal effects and increasing ablation uniformity.

Keywords: Femtosecond laser, Ablation, Polymers, High-frequency, Thermal effects, Absorption mechanism.

1 Introduction

Polymers have become essential materials over the last years. The presence of polymers in an endless number of disciplines, such as technological and medical devices, domestic appliances, food industry or aeronautics [1–3] has been increased because of their notable qualities and their competitive economical cost.

Three of the most commonly used polymers are poly (vinyl chloride) (PVC), poly(ethylene terephthalate) (PET) and polypropylene (PP). PVC is an amorphous polymer, whereas PET and PP are semi-crystalline polymers. These materials can be found in a vast number of ordinary objects [4–6]. Nevertheless, an important application of these polymers is their use in the fabrication of flexible electronical and photonic devices via ultrafast laser techniques [7, 8].

The use of ultrafast laser techniques for manufacturing micro devices has been widely investigated. Several valuable devices have been fabricated, such as microlenses, waveguides, diffractive gratings or microfluidic channels [9–16].

Femtosecond laser sources allow to deliver high intensities on the surface of the materials that produce non-linear absorptions restricted to the irradiated volume [17–20]. This enables to process materials that are transparent to lower light intensities through multiphoton absorption mechanisms. For this reason, ultrashort laser irradiation has become an exceptional tool for tunable material micro-processing [20].

The control of laser parameters is key for achieving a proper processing of the materials. The relation between the irradiation wavelength and the material bandgap becomes crucial because these parameters determinate the dominant absorption mechanism [20]. For higher wavelengths the amount of simultaneously absorbed photons must be greater, reducing the processing efficiency. If the wavelength is such that the photon energy is similar to the material bandgap, better processing results are expected to be obtained.

Another important parameter is the repetition rate. The short processing times demanded by the industry can be achieved with high repetition rate processing. When high repetition rate pulses are irradiated, time between pulses becomes shorter, resulting in shortened processing times and presenting a notable advantage for production purposes [15, 16]. The advantages of high repetition rate processing have been observed in several materials [21, 22], obtaining more uniform ablation and a debris reduction

* Corresponding author: dan.puerto@ua.es

in the surroundings of the ablation area. However, a wide range of repetition rate analysis is needed for understanding the impact of repetition rate in ablation efficiency and for controlling the processing outcomes.

We study the effects of processing three polymers with different thermal properties (PVC, PET and PP) using femtosecond laser irradiation for three different wavelengths ($\lambda = 343$ nm, 515 nm and 1030 nm) and a wide range of repetition rates (from 10 kHz to 1 MHz), providing a complete study of the processing of these materials under different laser conditions. This investigation highlighted the influence of the dominant absorption mechanism in achieving effective material processing. By adjusting the repetition rates, it was possible to precisely control and vary the ablation depths and diameters of the modifications at the micron level. An explanation for the results can be given by considering the connection between heat diffusion and repetition rate.

2 Experimental

The laser set up includes an NKT aeroPULSE FS50 fiber laser that emits 450 fs laser pulses with an average maximum power of 50 W at the central wavelength of $\lambda = 1030$ nm. Second order ($\lambda = 515$ nm) and third order ($\lambda = 343$ nm) harmonics can also be generated through a nonlinear crystal device. Repetition rates can be selected in a range between 500 Hz and 2 MHz for each wavelength. The working fluences are 1.70 J/cm^2 for $\lambda = 1030$ nm and 1.40 J/cm^2 for $\lambda = 515$ nm and 343 nm. We selected these fluence values based on the single pulse modification threshold for $\lambda = 515$ nm, which is slightly below 1.40 J/cm^2, according to our fluence tests. This choice ensures that all the emitted pulses are capable of modifying the surface of the materials. Ideally, to assess whether the absorption mechanism significantly influences the process, irradiation at $\lambda = 343$ nm, 515 nm and 1030 nm should occur at identical fluence values. This approach allows that any differences observed in the results for each wavelength to be attributed to the variations in the absorption of the materials at each wavelength. However, $\lambda = 1030$ nm required a higher fluence to induce significant modifications on the surface of the materials. Consequently, the fluence was increased to 1.70 J/cm^2 for this wavelength.

The system includes a scanner that controls the X–Y position of the laser beam, allowing to process different geometries on the material samples. The velocity of the scanner can be set between 1 mm/s and 5 m/s. The laser beam is focalized by a f-theta lens leading to 15 µm, 9 µm and 7 µm radii at $1/e^2$ for $\lambda = 1030$ nm, 515 nm and 343 nm, respectively. The radii sizes have been determined by the method proposed by Liu et al. [23]. A depiction of the experimental system is presented in Figure 1.

The polymer samples are 300 µm thick films of PVC, PET and PP. The absorbance spectra of these materials are presented in Figure 2. As it can be seen, the three polymers present an absorption peak for $\lambda \leq 300$ nm. Absorption for $\lambda = 343$ nm is slightly higher than for $\lambda = 515$ nm as seen in Table 1. However, for higher wavelengths absorption is expected to be lower. A simple way for comparing the absorption efficiency for the three wavelengths is by the estimation of the bandgap. This estimation can be performed from the slope of these peaks. The bandgap value is approximated to the wavelength value at which a straight line with this slope and situated on the top of the peak intersects the abscises axis. The bandgap estimations can be observed in Table 1. Regarding the low absorption of the three materials at the working wavelengths and the high intensities that are provided by an ultrafast laser source, multiphoton absorption is expected to be the dominant absorption mechanism for $\lambda = 1030$ nm and $\lambda = 515$ nm processing. Considering the bandgap energies, the energy of each wavelength can allow us to estimate the number of simultaneous photons that are required to be absorbed. The photon energy for $\lambda = 1030$ nm is 1.20 eV, for $\lambda = 515$ nm is 2.41 eV and for $\lambda = 343$ nm is 3.61 eV. These findings suggest that, across all the three materials, at least 4 photons are needed to be absorbed simultaneously for $\lambda = 1030$ nm, whereas only 2 coincident photons are necessary for $\lambda = 515$ nm. In the case of 343 nm irradiation, it is plausible that two-photon absorption may interplay with linear absorption. This phenomenon could influence the material processing outcomes, as explained in the subsequent sections.

Thermal properties of the three materials have been analysed too (see Supplementary material). Glass transition (T_g), melting (T_m), decomposition (T_d) temperatures and heat capacity at T_d are determined from Modulated Differential Scanning Calorimetry (MDSC) and Thermogravimetry (TG). The results are also presented in Table 1.

Optical characterization system is composed by an Olympus IX73 microscope with 10×/0.30, 20×/0.45, 50×/0.80 and 100×/0.90 MPlanFLN objectives. The ablation depths were measured using this microscope, focusing on the surface of the material and on the deepest region of the induced ablations. The differences between the reading on the micrometric stage on the material surface and on the ablated regions were recorded as the depth measurements. We conducted multiple measurements of the ablation depth for each line to minimize errors. The ablation and modified widths were determined using microscopic images and the micron/pixel calibration that was established.

3 Results and discussion

3.1 Overview

Different series of irradiated lines with different number of pulses per spot-area were processed on the three polymer surfaces at $\lambda = 1030$ nm with a fluence of 1.70 J/cm^2 and at $\lambda = 515$ nm and 343 nm with a fluence of 1.40 J/cm^2 for both wavelengths. Each series contains irradiations with different values of repetition rate and scanning velocity. These two parameters were varied in order to obtain a constant number of pulses. Therefore, each sequence consists on lines with the same number of pulses per spot-area, but each line is produced with a different value of repetition rate.

The fact of varying the repetition rate values alters the heat diffusion mechanism. For higher repetition rates, time

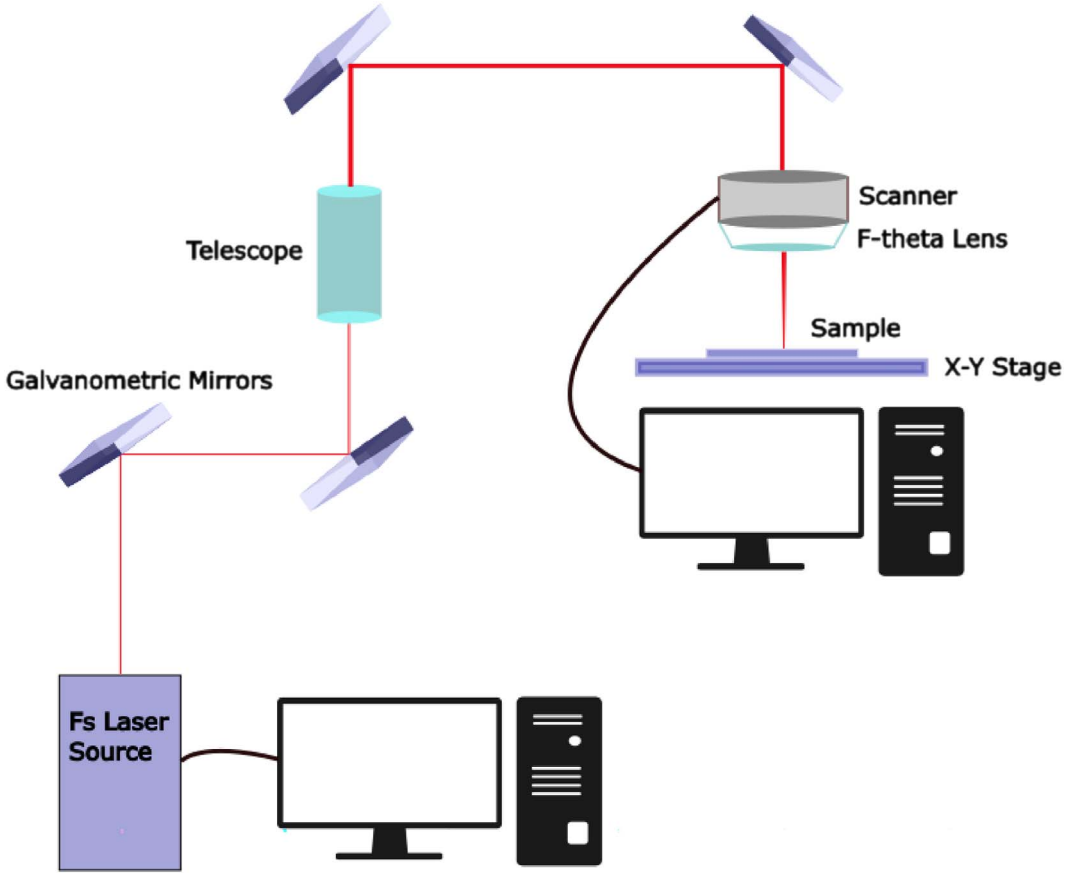

Fig. 1. Sketch of the used experimental setup.

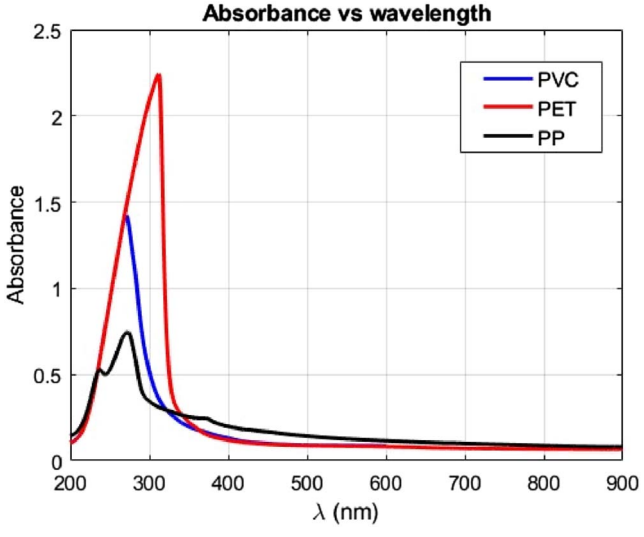

Fig. 2. Absorbance spectra for PVC, PET and PP.

between pulses is reduced, so it is more difficult for the material to spread the induced heat on its surface, leading to higher temperatures that can produce greater changes in the materials. After the last pulse impinges the material, heat diffusion becomes dominant and the high temperatures that have been reached on the irradiated area are able to enlarge the modified region. Increasing the number of overlapping pulses and the delivered pulse energy also causes a greater increase of the temperature. However, a finer control of the material temperature can be achieved by varying repetition rates while fluence and number of pulses are unchanged.

For this reason, in the following analysis, fluence values and number of pulses are set constant for each repetition rate-varying irradiation series. Consequently, the differences between modified volumes on lines of the same series are attributed to effects related to the thermal characteristics of the materials.

3.2 Results for $\lambda = 1030$ nm

Ablation is not the dominant consequence of processing these polymers with $\lambda = 1030$ nm irradiations. As it was mentioned above, considering the bandgaps of the materials and the photon energies for this wavelength, at least 4 photons are required to be absorbed at the same time for the three materials for this wavelength. This implies that absorption is less efficient for this wavelength than for $\lambda = 515$ nm and 343 nm and, as a consequence, lower temperatures will be reached. This fact is evinced in the following results.

PVC and PET present analogous effects at this wavelength, but at different number of pulses and repetition rate

Table 1. Estimated bandgaps, absorbance for $\lambda = 343$ and for $\lambda = 515$ nm, glass transition temperatures (T_g), melting temperatures, (T_m), decomposition temperatures (T_d) and heat capacity at 25 °C and at T_d for PVC, PET and PP.

Polymer	Bandgap (eV)	Absorbance 343 nm	Absorbance 515 nm	T_g (°C)	T_m (°C)	T_d (°C)	C_p at 25 °C (J/kg K)	C_p at T_d (J/kg K)
PVC	3.95	0.216	0.090	72.29	–	225	690	1568
PET	3.80	0.257	0.087	75.55	245.45	349	827	1979
PP	4.00	0.262	0.138	<0	157.96	320	1181	2928

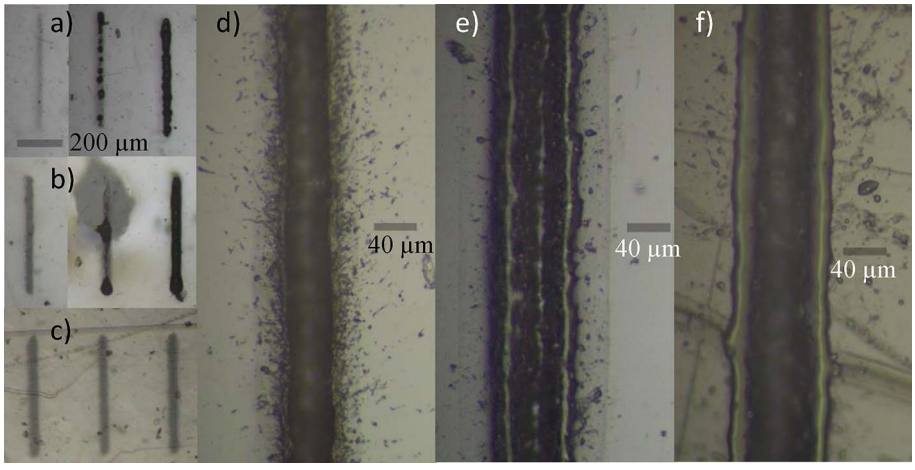

Fig. 3. (a) PVC irradiations at 1030 nm with $N = 25$, 40 and 65 pulses/spot-area from left to right and $\boldsymbol{f} = 5$ kHz. (b) PET irradiations at 1030 nm with $N = 60$ pulses/spot-area and $\boldsymbol{f} = 2.5$ kHz, 110 and 125 pulses/spot-area and $\boldsymbol{f} = 100$ kHz from left to right. (c) PP irradiations at 1030 nm with $N = 125$ pulses/spot-area and $\boldsymbol{f} = 200$, 250 and 300 kHz from left to right. The scale bar shown in (a) is applicable to (b) and (c) too. (d) PVC irradiation at 1030 nm with $N = 125$ pulses and $\boldsymbol{f} = 1$ MHz. (e) PET irradiation at 1030 nm with $N = 250$ pulses and $\boldsymbol{f} = 100$ kHz. (f) PP irradiation at 1030 nm with $N = 400$ pulses/spot-area and $\boldsymbol{f} = 1$ MHz. All the presented irradiations were performed at a fluence value of 1.70 J/cm^2.

values. For lower number of pulses/spot-area (about 25 for PVC and 60 for PET) only reflectivity changes are observed on the material surface, as seen in the left lines of Figures 3a and 3b. Above these values, thermal effects extended outside the irradiation area emerge. As the number of pulses increases (40–65 for PVC and 80–125 for PET) ablation appears and mixes with those extended thermal effects (see the central lines of Figs. 3a and 3b). Furthermore, burning traces are observable on the surroundings of the irradiated areas, as depicted in Figure 3b. It can be noted that when fluence is lower than the ablative threshold for a certain wavelength, surrounding heat transfer is increased. When ablation is achieved, a greater portion of the transferred energy is used to increase the ablated depth, leading to more restricted area effects. These extended effects are more prevailing for PET than for PVC. For higher number of pulses (65 for PVC and 125 for PET) ablation dominates as it can be noted for the right lines in Figures 3a and 3b. However, for the laser conditions for which ablation is achieved, the uniformity of the lines is quite low and the presence of debris is notable, even for high repetition rate irradiated lines, as seen in Figures 3d and 3e.

The differences between the required number of pulses for ensure ablation between PVC and PET might be explained regarding the heat capacity values at 25 °C and at T_d that can be seen in Table 1. It can be noted that PET exhibits a slightly greater heat capacities at both temperatures compared to PVC. This suggests that PET requires more energy for elevating its temperature than PVC. This disparity is increased for higher temperatures, as heat capacity differences between both materials are higher at T_d than at 25 °C. As a consequence, this may challenge ablation for PET. The smaller T_d presented by PVC also can benefit ablation compared to PET. The extended thermal effects can be explained by the glass-rubbery phase transitions that suffer PVC and PET when temperature is above 72 °C and 76 °C, respectively (see Tab. 1). These phase changes increase the volume of the material, obtaining thermal effects that are propagated outside the irradiation area. Then, rubbery state resolidifies and causes a change in the refractive index [13, 15, 20, 24, 25], as it is shown in Figure 3d.

On the other hand, PP shows a different behaviour. A higher number of pulses and repetition rate (1000 pulses and 100 kHz or 400 pulses and 1 MHz) is required to ensure a complete ablation. This can be understood regarding the notably higher heat capacity values at 25 °C and, especially, at T_d presented by this material (see Tab. 1). At lower number of pulses (about hundreds of pulses), non-extended reflectivity changes are the main consequences of processing this material, as it is shown in Figure 3c.

The lack of huge external thermal effects (as contrary as in the case of PVC and PET) may be related to the absence of glass-rubbery transition for PP at temperatures above 0 °C. Therefore, PP is already at rubbery state at ambient temperature, and this transition does not occur when the material is processed. Additionally, two homogeneous bleaching regions are discernible on the bordering of the ablation area in Figure 3f. These modifications are attributed to the flow of material that experienced a melting transition. Similar bleaching effects can also be noted on the edges of the ablated lines in PET, as seen in Figure 3e. These modifications are also attributed to the melting transition suffered by PET. The smaller size of bleaching observed in PET correlates with its higher melting temperature (245 °C) compared to PP (158 °C), as presented in Table 1. The lack of these regions for PVC correlates with the absence of melting transition for this material. The homogeneity of the ablation lines processed at high number of pulses and repetition rates is superior to that of PVC and PET, but it remains not entirely satisfactory for PP, as seen in Figure 3f.

The results of processing these three polymers with 1030 nm laser irradiation indicate that ablation is not achieved across all the studied laser conditions. High number of pulses and repetition rates are required to ensure ablation, especially for PP. Otherwise, only reflectivity changes or non-uniform ablation mixed with thermal effects appear. Even when ablation is accomplished, the resulting lines exhibit low uniformity and homogeneity. Consequently, processing these materials with 1030 nm under these laser conditions represents a less controllable process, obtaining non-optimal outcomes.

3.3 Results for $\lambda = 515$ and 343 nm

The consequences of processing these materials using $\lambda = 515$ nm and 343 nm exhibit similarities. Contrary to the $\lambda = 1030$ nm case, where ablation induced on the surface of the three polymers is less dominant, ablation is achieved for all the investigated repetition rates and materials for both wavelengths.

This fact aligns with the absorption spectra and bandgaps characteristics of the polymers (see Fig. 2 and Tab. 1). As it was discussed above, two-photon absorption dominates for $\lambda = 515$ nm, and appears combined with single photon absorption for $\lambda = 343$ nm, contrasting to the four photons that are needed for $\lambda = 1030$ nm. Consequently, absorption is more efficient for $\lambda = 515$ nm and 343 nm, generating higher temperatures on the material surfaces, that can exceed the decomposition temperature of the materials (T_d, see Tab. 1), enabling ablation. It must be emphasized that ablation has been achieved for a smaller number of pulses and fluence for $\lambda = 515$ nm and 343 nm than for $\lambda = 1030$ nm, underscoring the influence of the absorption mechanism on the processing efficiency.

However, despite absorbance is higher for $\lambda = 343$ nm compared to $\lambda = 515$ nm, there are differences in the pulse energy distribution of each wavelength. Specifically, the waist radius for $\lambda = 515$ nm is 9 μm at $1/e^2$, whereas the value for $\lambda = 343$ nm is 7 μm. As a consequence of the lower absorbance for 515 nm for the three materials, a greater skin depth is expected for this wavelength processing, originating greater optical penetration depths. These facts could affect to the ablation depth and the modification widths, as detailed in this section.

To compare the differences between these wavelengths and materials, ablation depths and modification diameters for 150 pulses/spot-size irradiated lines series were measured across repetition rates ranging from 10 kHz to 1 MHz.

As it can be observed in Figures 4, 5, 6a and 6b, modified areas increase with repetition rate for the repetition rates that are shown in the images. The homogeneity of the processed lines is increased too as repetition rate is risen up. In Figures 4, 5, 6c and 6d 1 MHz irradiated lines are depicted, denoting a notable homogeneity. In contrast to the 1030 nm case (Figs. 3d–3f), the uniformity of the processed lines is remarkably enhanced for 515 nm and 343 nm processing, achieving more favoured outcomes for these two wavelengths.

Figures 4, 5, 6a and 6b also indicate that PVC and PET present greater modified widths and reflectivity changes in the ablation surroundings than PP. PP does not present these reflectivity variations. The two observable bleaching regions on the bordering of the ablation area are also attributed to flowed material, as explained in the previous subsection. In order to clarify the specific modification region, three different parameters are analysed for each material and wavelength: ablation depths, ablation diameters and extended diameters. The ablation depth is characterized as the maximum profundity of the removed volume. The ablation diameter denotes the horizontal width of the darkened ablation region. The extended diameters for PVC and PET are defined as the total reflectivity change widths, while for PP the extended diameters refer to the maximum distance between the external bleaching regions. An illustration of the diameters definitions is given in Figures 4, 5 and 6d.

The presence of reflectivity changes that expand the extended diameters for PVC and PET might be attributed to the phase changes experienced by these materials, as explained in the previous section. The glass transition suffered by PVC and PET at $T_g \sim 75$ °C triggers the enlargement of the modified region and the refractive index variation due to the volume increase during this phase transition. Nevertheless, PP glass transition occurs at temperatures below to 0 °C. As a consequence, this transition will not occur when PP is irradiated. This also explains the larger extended diameters in PVC and PET compared to PP.

PVC and PET also exhibit greater ablation depths than PP. This disparity might also be explained regarding the heat capacity values that can be seen in Table 1, as explained above. The greater PP heat capacities at indicate that this material presents a higher resistance for increasing its temperature compared to PVC and PET, challenging ablation.

Figures 4, 5, 6e and 6f demonstrate that ablation depths and extended and ablation diameters increase with repetition rate, occurring up to approximately 100 kHz for both wavelengths and the three materials. Beyond this range, these three parameters saturate, remaining nearly constant or even decreasing, as seen in the extended diameter for PVC and PET.

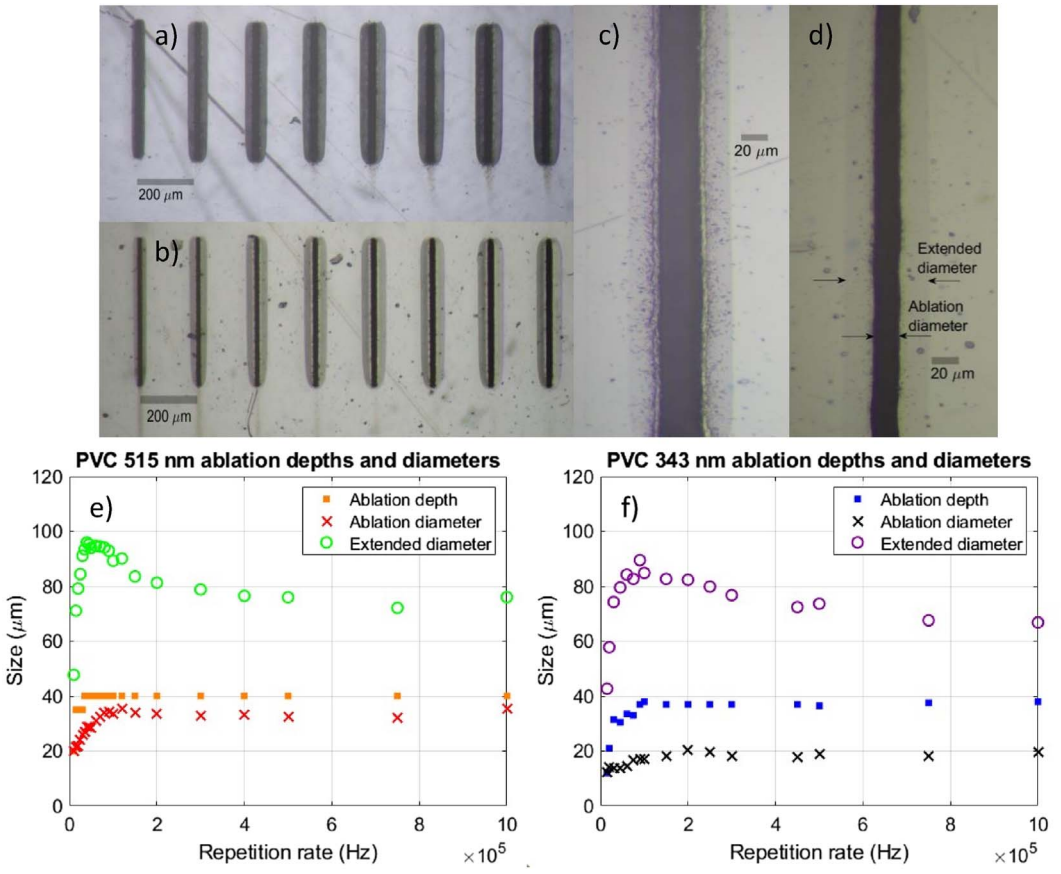

Fig. 4. (a) PVC irradiations at 515 nm with $N = 150$ pulses/spot-area and $\boldsymbol{f} = 10$–45 kHz increasing from left to right. (b) PVC irradiations at 313 nm with $N = 150$ pulses/spot-area and $\boldsymbol{f} = 15$–100 kHz increasing from left to right. (c) PVC 1 MHz irradiation with $N = 150$ pulses/spot-area and 515 nm. (d) PVC 1 MHz irradiation with $N = 150$ pulses/spot-area and 343 nm. (e) PVC measured irradiated lines ablation depth, ablation diameter and extended diameter for $N = 150$/spot-area at 515 nm as functions of repetition rate. (f) PVC measured irradiated lines ablation depth, ablation diameter and extended diameter for $N = 150$/spot-area at 343 nm as functions of repetition rate. All the presented irradiations were performed at a fluence value of 1.40 J/cm^2.

In this sense, two remarkable consequences of processing these materials must be emphasized: Firstly, by varying the repetition rate at a constant fluence and number of pulses a tunable micron-scale depths and modified diameters can be achieved. Furthermore, high repetition rate ablation not only contribute to a higher line uniformity, but also leads to a diminution of extended thermal effects for PVC and PET, enabling more precise processing.

The saturation phenomenon can be understood concerning the thermal diffusivity of the materials and the time between laser pulses. When a pulse impinges the surface of the material, temperature is increased in the irradiated area. At lower repetition rate values (larger time between pulses) materials are able to revert to their pre-pulse temperature, since time between pulses is greater than the diffusion time of the material. However, as repetition rate increases, the reduced time between pulses limits heat diffusion efficiency, leading to cumulative heat effects, that produce a significant rise of the material temperature. The critical repetition rate that supposes the entry into the heat accumulation regimes can be estimated as [13, 20, 26]

$$f_C = \frac{D}{4\omega^2}, \tag{1}$$

where D is the thermal diffusivity and ω represents the laser radius at the focal plane. For thermal diffusivities $D \sim 8 \cdot 10^{-8}$ m^2/s for the three polymers, and $\omega = 7$ μm for 343 nm irradiations and $\omega = 9$ μm for 515 nm, the critical repetition rate is $f_C \sim 250$–400 Hz. Notably, the working repetition rates exceed f_C in all the cases, indicating that all the lines have been irradiated on the heat accumulation regime. Consequently, the increase in ablation depths and diameters with repetition rate can be attributed to the heat accumulation effects that become more relevant as the repetition rate is increased.

Nevertheless, for repetition rates higher than 100 kHz, approximately, no further increments are noted for these three parameters, as illustrated in Figures 4, 5, 6e and 6f. This saturation is attributed to the fact that heat diffusion efficiency is reduced for this range of repetition rates. At these repetition rates, time between pulses becomes so small that temperature of the material remains essentially

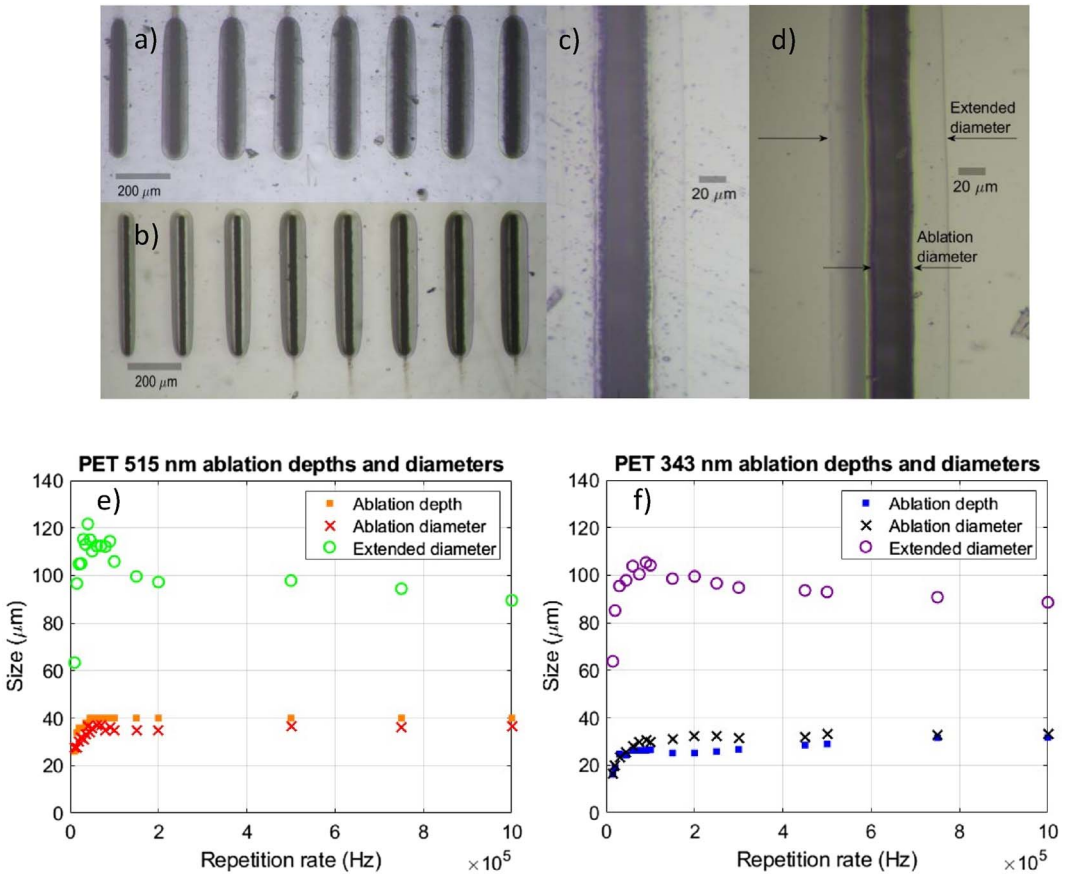

Fig. 5. (a) PET irradiations at 515 nm with $N = 150$ pulses/spot-area and $\boldsymbol{f} = 10$–45 kHz increasing from left to right. (b) PET irradiations at 313 nm with $N = 150$ pulses/spot-area and $\boldsymbol{f} = 15$–100 kHz increasing from left to right. (c) PET 1 MHz irradiation with $N = 150$ pulses/spot-area and 515 nm. (d) PET 1 MHz irradiation with $N = 150$ pulses/spot-area and 343 nm. (e) PET measured irradiated lines ablation depth, ablation diameter and extended diameter for $N = 150$/spot-area at 515 nm as functions of repetition rate. (f) PET measured irradiated lines ablation depth, ablation diameter and extended diameter for $N = 150$/spot-area at 343 nm as functions of repetition rate. All the presented irradiations were performed at a fluence value of 1.40 J/cm^2.

constant until the next pulse arrives. As a consequence, material temperatures will not grow significantly if time between pulses is reduced. This occurs when time between pulses becomes considerably smaller than the diffusion time of the material. It must be noted that for 100 kHz, time between pulses $\left(t_{\text{bp}} = \frac{1}{f} = 10^{-5}\,\text{s}\right)$ is between 250 and 400 times smaller than the time associated to the critical repetition rate $\left(t_c = \frac{1}{f_c} \sim 2.5 \cdot 10^{-3} - 4 \cdot 10^{-3}\,\text{s}\right)$. This reduction of the time between pulses could enable the saturation effect.

However, this reasoning does not explain the reduction of the external diameter size seen in PVC and PET after reaching a maximum for repetition rates near to 100 kHz (see Figs. 4, 5e and 5f). This phenomenon can be attributed to the way absorbed energy is distributed among different processes. Some part of the absorbed energy is spent for ablating and evaporating the material, another part remains in the vapor as kinetic energy and the residual heat is located in the bulk and the surface of the material, surrounding the ablation volume [27]. Initially, as repetition rate increases, temperatures rise up, increasing the amount of energy available for heat diffusion because a smaller portion of the absorbed energy is devoted to ablation. Diffusion elevates the temperature on the ablation surroundings and, if temperature becomes greater than T_g the extended diameter will be enlarged. However, at higher repetition rates, temperatures may become sufficient for achieving greater ablation volumes, reducing the available residual energy for heat diffusion [22], resulting in a diminution of the external diameters for both materials.

Considering the ablation diameters saturation repetition rates and the maximum extended diameters repetition rates the transition between the thermal effects dominating regime and the ablation regime can be estimated.

For PVC, the maximum external diameter is originated at 40 kHz for 515 nm and at 90 kHz for 343 nm irradiation. The saturation of the ablation diameters is produced at 70 kHz for 515 nm irradiations and at 90 kHz for 343 nm processing. This indicates that the transition between both regimes is produced between 40 and 70 kHz for 515 nm and about 90 kHz for 343 nm for this polymer.

In the case of PET, the greatest extended diameter is obtained at 30 kHz for 515 nm and at 60 kHz for 343 nm. Ablation diameters saturate at 60 kHz for 515 nm and at

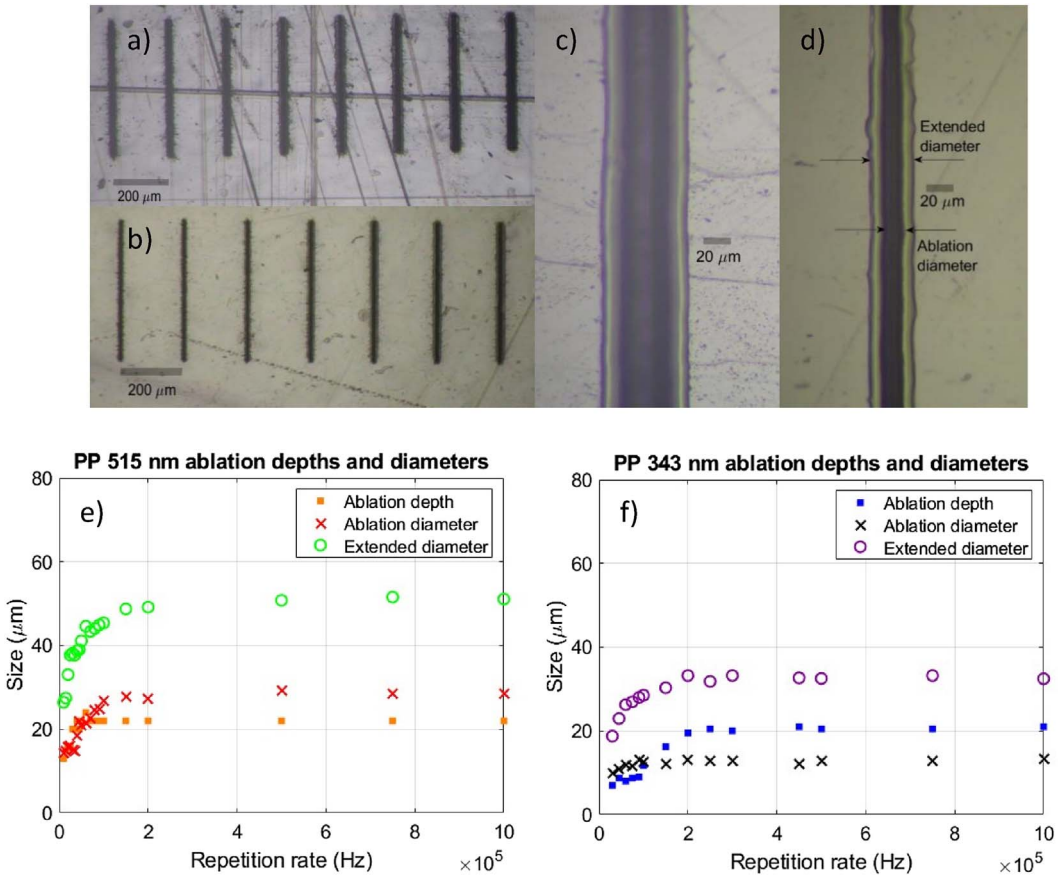

Fig. 6. (a) PP irradiations at 515 nm with N = 150 pulses/spot-area and $\boldsymbol{f}$ = 10–45 kHz increasing from left to right. (b) PP irradiations at 313 nm with N = 150 pulses/spot-area and $\boldsymbol{f}$ = 15–100 kHz increasing from left to right. (c) PP 1 MHz irradiation with N = 150 pulses/spot-area and 515 nm. (d) PP 1 MHz irradiation with N = 150 pulses/spot-area and 343 nm. (e) PP measured irradiated lines ablation depth, ablation diameter and extended diameter for N = 150/spot-area at 515 nm as functions of repetition rate. (f) PP measured irradiated lines ablation depth, ablation diameter and extended diameter for N = 150/spot-area at 343 nm as functions of repetition rate. All the presented irradiations were performed at a fluence value of 1.40 J/cm^2.

Table 2. Maximum extended diameter, extended diameter at 1 MHz, ablation diameter at 1 MHz and ablation depth at 1 MHz for PVC, PET and PP at 515 nm and 343 nm irradiation.

Polymer and wavelength	Max. extended diameter	Extended diameter at 1 MHz	Ablation diameter at 1 MHz	Ablation depth at 1 MHz
PVC (515 nm)	96 μm	76 μm	36 μm	40 μm
PVC (343 nm)	90 μm	67 μm	20 μm	38 μm
PET (515 nm)	122 μm	90 μm	37 μm	40 μm
PET (343 nm)	105 μm	89 μm	33 μm	33 μm
PP (515 nm)	51 μm	51 μm	29 μm	22 μm
PP (343 nm)	33 μm	33 μm	13 μm	21 μm

75 kHz for 343 nm. This points that, for this material the transition is produced between 30 kHz and 60 kHz for 515 nm and between 60 kHz and 75 kHz for 343 nm.

PP does not exhibit a decrease of the extended diameters for repetition rates greater than 100 kHz. Its extended and ablation diameters reach a maximum at 90 kHz for 515 nm irradiation, remaining constant as the repetition rate is increased. The same behaviour is found for 343 nm, obtaining a saturation for extended and ablation diameters at 150 kHz. This behaviour aligns with the absence of extended thermal effects due to the lack of the glass transition during PP irradiation and confirms that the two bleaching regions are due to deposited material.

Being conscious of the repetition rate ranges where ablation predominates over thermal effects becomes crucial for acquiring control over material processing. A strategic

convenient repetition rate can be selected in order to obtain the desired outcome after material irradiation.

There are also differences between both processing wavelengths for the three materials as shown in Table 2. Greater extended and ablation diameters are attained with 515 nm irradiations. The disparities between the maximum extended diameters at 515 nm and 343 nm are significant across the three materials, obtaining significantly greater modification areas at 515 nm. Differences in ablation diameter sizes between 515 nm and 343 nm irradiations at 1 MHz are also notable (1.8 ratio for PVC, 1.1 ratio for PET and 2.2 ratio for PP). Concerning ablation depth, comparable values are obtained for the three materials at both wavelengths: PVC ratio 1.1, PET ratio 1.2 and PP ratio 1. This indicates that greater volumes are ablated with 515 nm compared to 343 nm: 1.9 ratio for PVC, 1.4 ratio for PET and 2.3 ratio for PP.

In terms of the importance of achieving ablations with greater volumes and smaller diameters for acquiring control on the ablation area, it can be noted that, although bigger volumes are removed with 515 nm, the fact that the ablation diameters are smaller for the three materials at 343 nm indicates that sharper ablations can be achieved with 343 nm processing.

These results can be understood considering the differences between the materials absorption and the distinct radius waists at each wavelength. The greater ablation and extended diameters at 515 nm are attributed to the larger radius waists for this wavelength. Nevertheless, the fact that comparable ablation depths are achieved for both wavelengths is a consequence of the higher absorption of the three materials at 343 nm. Thus, generally, lower waist radii and greater absorptions benefit controllable ablation, increasing the processing precision.

4 Conclusions

The behaviour of three commercial polymers has been analysed under three different wavelength ($\lambda = 343$ nm, 515 nm and 1030 nm) femtosecond laser irradiation for a wide range of repetition rates. The results point that 1030 nm irradiations are not efficient at our working fluence because for this wavelength, at least 4 photons are demanded to be absorbed at the same time for exceeding the bandgap energy for the three materials. As a consequence, non-uniform ablation, reflectivity changes and undesired extended thermal effects accompanied by burning traces are achieved at this wavelength. Conversely, two photon absorption is the main absorption mechanism for 515 nm and 343 nm processing for the three polymers, leading to a more suitable processing for which ablation is the main outcome. This fact highlights the significance of the dominant absorption mechanism for processing efficiency. For the latter two wavelengths ablation depths and modified diameters are measured, observing an increase of this parameters with repetition rate up to values around 100 kHz, and originating a saturation or even a diminution on the extended diameters for PVC and PET. This indicates that tunable depths and modified areas at the micron level can be achieved by varying repetition rate at constant fluence and number of pulses. More suitable results are attained at high repetition rates, leading to more uniform lines for all the three materials and reduced extended diameters, particularly for the case of PVC and PET. The saturation effect can be understood considering the relation between the thermal diffusivity of the materials and the time between pulses. The decreasing of the extended diameters for PVC and PET can be explained regarding the distribution of the absorbed energy among ablation processes and heat diffusion. Regarding ablation precision, significant sharper ablations at 343 nm are achieved compared to 515 nm.

Supplementary material

Figure S1: MDSC curves for PVC (a), PET (b) and PP (c). Tg, and Tm are indicated with arrows. Thermogravimetry (TG, in black), derivative thermogravimetric curves (DTG, in blue) and decomposition temperatures (in red) for PVC (d), PET (e) and PP (f).

The supplementary material of this article are available at https://jeos.edpsciences.org/10.1051/jeos/2024021/olm.

Funding

The work was supported by the "Generalitat Valenciana" (IDIFEDER/2021/014 cofunded by FEDER EU program, project PROMETEO/2021/006, and INVESTIGO program (INVEST/2022/419) financed by Next Generation EU), "Ministerio de Ciencia e Innovación" of Spain (projects PID2021-123124OB-I00; PID2019-106601RB-I00), by "Universidad de Alicante" (UATALENTO18-10). APB thanks the "Ministerio de Ciencia e Innovación" for the grant (PRE2022-105016).

Conflicts of interest

The authors declare that they have no known competing financial interests or personal relationships that could have appeared to influence the work reported in this paper.

Data availability statement

No data was used for the research described in the article.

Author contribution statement

A.P. Bernabeu: Writing – review & editing, writing – original draft, investigation, data curation. G. Nájar: Investigation, software, data curation. A. Ruiz: Investigation, data curation. J.C. Bravo: Investigation, software. M.G. Ramirez: Methodology, investigation, conceptualization. S. Gallego: Writing – review & editing, writing – original draft, resources, conceptualization, funding acquisition. A. Márquez: Writing – original draft, investigation, conceptualization, funding acquisition. D. Puerto: Writing – review & editing, writing – original draft, supervision, investigation, data curation, conceptualization.

References

1 Modjarrad K., Ebnesajjad S. (2014) *Handbook of polymer applications in medicine and medical devices*, 1st ed, Elsevier, San Diego, CA, USA.
2 Ramakrishna S., Mayer J., Wintermantel E., Leong K.W. (2001) Biomedical applications of polymer-composite

materials: A review, *Compos. Sci. Technol.* **61**, 9, 1189–1224. https://doi.org/10.1016/S0266-3538(00)00241-4.
3 Scholz C. (2017) *Polymers for biomedicine: Synthesis, characterization, and applications*, 1st ed., John Wiley & Sons, Hoboken, NJ, USA.
4 Leadbitter J., Day J.A., Ryan J.L. (1997) *PVC: Compounds, processing and applications*, Rapra Technology Ltd, Shawbury, UK.
5 Maddah H.A. (2016) Polypropylene as a promising plastic: A review, *Am. J. Polym. Sci.* **6**, 1, 1–11.
6 Carr C.M., Clarke D.J., Dobson A.D.W. (2020) Microbial polyethilene terephthalate hydrolases: Current and future perspectives, *Front. Microbiol.* **11**, 1–23.
7 Zacharatos F., Makrygianni M., Geremina R., Biver E., Karnakis D., Leyder S., Puerto D., Delaporte P., Zergioti I. (2016) Laser direct write micro-fabrication of large area electronics on flexible substrates, *Appl. Surf. Sci.* **374**, 117–123. https://doi.org/10.1016/j.apsusc.2015.10.066.
8 Sun Y., Rogers J.A. (2007) Inorganic semiconductors for flexible electronics, *Adv. Mater.* **19**, 15, 1897–1916. https://doi.org/10.1002/chin.200739224.
9 Xu M., Xue Y., Li J., Zhang L., Lu H., Wang Z. (2023) Large-area and rapid fabrication of a microlens array on flexible substrate for an integral imaging 3D display, *ACS Appl. Mater. Interfaces* **15**, 10219–10227. https://doi.org/10.1021/acsami.2c20519.
10 Zheng C., Hu A., Kihm K.D., Ma Q., Li R., Chen T., Duley W.W. (2015) Femtosecond laser fabrication ofcavity micro-ball lens (CMBL) inside a PMMA substrate for super-wide angle imaging, *Small* **11**, 25, 3007–3016. https://doi.org/10.1002/smll.201403419.
11 Puerto D., Biver E., Alloncle A.-P., Delaporte P. (2016) Single step high-speed printing of continuous silver lines by laser-induced forward transfer, *Appl. Surf. Sci.* **374**, 183–189. https://doi.org/10.1016/j.apsusc.2015.11.017.
12 Bollgruen P., Wolfer T., Gleissner U., Mager D., Megnin C., Overmeyer L., Hanemann T., Korvink J.G. (2017) Ink-jet printed optical waveguides, *Flex. Print. Electron.* **2**, 4, 045003. https://doi.org/10.1088/2058-8585/aa8ed6.
13 Sola D., Vázquez de Aldana J.R., Artal P. (2020) The role of thermal accumulation on the fabrication of diffraction gratings in ophthalmic PHEMA by ultrashort laser direct writing, *Polymers* **12**, 12, 2965. https://doi.org/10.3390/polym12122965.
14 Suriano R., Kuznetsov A., Eaton S.M., Kiyan R., Cerullo G., Osellame R., Chichkov B.N., Levi M., Turri S. (2011) Femtosecond laser ablation of polymeric substrates for the fabrication of microfluidic channels, *Appl. Surf. Sci.* **257**, 14, 6243–6250. https://doi.org/10.1016/j.apsusc.2011.02.053.
15 Eaton S.M., Zhang H., Herman P.R., Yoshino F., Shah L., Bovatsek J., Arai A.Y. (2005) Heat accumulation effects in femtosecond laser-written waveguides with variable repetition rate, *Opt. Exp.* **13**, 12, 4708–4716. https://doi.org/10.1364/opex.13.004708.
16 Eaton S.M., Zhang H., Ling M., Li J., Chen W.-J., Ho S., Herman P.R. (2008) Transition from thermal diffusion to heat accumulation in high repetition rate femtosecond laser writing of buried optical waveguides, *Opt. Exp.* **16**, 13, 9443–9458. https://doi.org/10.1364/oe.16.009443.
17 Lenzner M. (1999) Femtosecond laser-induced damage of dielectrics, *Int. J. Mod. Phys. B* **13**, 13, 1559–1578. https://doi.org/10.1142/s0217979299001570.
18 Stuart B.C., Feit M.D., Rubenchik A.M., Shore B.W., Perry M.D. (1995) Laser-induced damage in dielectrics with nanosecond to subpicosecond pulses, *Phys. Rev. Lett.* **74**, 12, 2248. https://doi.org/10.1103/physrevlett.74.2248.
19 Tien A.-C., Backus S., Kapteyn H., Murnane M., Mourou G. (1999) Short-pulse laser damage in transparent materials as a function of pulse duration, *Phys. Rev. Lett.* **82**, 19, 3883. https://doi.org/10.1103/physrevlett.82.3883.
20 Misawa H., Juodkazis S. (2006) *3D laser microfabrication*, Wiley-VCH Verlag, Weinheim, Germany.
21 Florian C., Fuentes-Edfuf Y., Skoulas E., Stratakis E., Sanchez-Cortes S., Solis J., Siegel J. (2022) Influence of heat accumulation on morphology debris deposition and wetting of LIPSS on steel upon high repetition rate femtosecond pulses irradiation, *Materials* **15**, 17468. https://doi.org/10.3390/ma15217468.
22 Kerse C., Kalaycıoğlu H., Elahi P., Çetin B., Kesim D.K., Akçaalan Ö., Yavaş S., Aşık M.D., Öktem B., Hoogland H., Holzwarth R., Ilday F.Ö. (2016) Ablation-cooled material removal with ultrafast bursts of pulses, *Nature* **537**, 7618, 84–88. https://doi.org/10.1038/nature18619.
23 Liu X., Du D., Mourou G. (1997) Laser ablation and micromaching with ultrashort laser pulses, *IEEE J. Quant. Electron.* **33**, 10, 1706–1716. https://doi.org/10.1109/3.631270.
24 Schaffer C.B., García J.F., Mazur E. (2003) Bulk heating of transparent materials using a high-repetition-rate femtosecond laser, *Appl. Phys. A* **76**, 351–354. https://doi.org/10.1007/s00339-002-1819-4.
25 Schaffer C.B., Brodeur A., García J.F., Mazur E. (2001) Micromachining bulk glass by use of femtosecond laser pulses with nanojoule energy, *Opt. Lett.* **26**, 2, 93–95. https://doi.org/10.1364/ol.26.000093.
26 Benayas A., Silva W.F., Ródenas A., Jacinto C., Vázquez de Aldana J., Chen F., Tan Y., Thomson R.R., Psaila N.D., Reid D.T., Torchia G.A., Kar A.K., Jaque D. (2011) Ultrafast laser writing of optical waveguides in ceramic Yb:YAG: A study of thermal and non-thermal regimes, *Appl. Phys. A* **104**, 301–309. https://doi.org/10.1007/s00339-010-6135-9.
27 Bauer F., Michalowski A., Kiedrowski T., Nolte S. (2015) Heat accumulation in ultra-short pulsed scanning laser ablation of metals, *Opt. Exp.* **23**, 2, 1035–1043. https://doi.org/10.1364/OE.23.001035.